Monthly Notices of the ROYAL ASTRONOMICAL SOCIETY

MNRAS **532,** 424–437 (2024) https://doi.org/10.1093/mnras/stae1524
Advance Access publication 2024 June 18

[O III] emission in $z \approx 2$ quasars with and without broad absorption lines

Matthew J. Temple [1,2]★ Amy L. Rankine [3] Manda Banerji [4] Joseph F. Hennawi [5,6] Paul C. Hewett [7] James H. Matthews [8] Riccardo Nanni,[5,6] Claudio Ricci [2,9] and Gordon T. Richards[10]

[1] *Centre for Extragalactic Astronomy, Department of Physics, Durham University, South Road, Durham DH1 3LE, UK*
[2] *Instituto de Estudios Astrofísicos, Universidad Diego Portales, Av. Ejército Libertador 441, Santiago 8370191, Chile*
[3] *Institute for Astronomy, University of Edinburgh, Royal Observatory, Blackford Hill, Edinburgh EH9 3HJ, UK*
[4] *School of Physics & Astronomy, University of Southampton, Southampton SO17 1BJ, UK*
[5] *Leiden Observatory, Leiden University, PO Box 9513, NL-2300 RA Leiden, the Netherlands*
[6] *Department of Physics, University of California, Santa Barbara, CA 93106, USA*
[7] *Institute of Astronomy, University of Cambridge, Madingley Road, Cambridge CB3 0HA, UK*
[8] *Department of Physics, Astrophysics, University of Oxford, Denys Wilkinson Building, Keble Road, Oxford OX1 3RH, UK*
[9] *Kavli Institute for Astronomy and Astrophysics, Peking University, Beijing 100871, China*
[10] *Department of Physics, Drexel University, 32 S. 32nd Street, Philadelphia, PA 19104, USA*

Accepted 2024 June 17. Received 2024 June 10; in original form 2023 September 29

ABSTRACT

Understanding the links between different phases of outflows from active galactic nuclei is a key goal in extragalactic astrophysics. Here, we compare [O III] λλ4960, 5008 outflow signatures in quasars with and without broad absorption lines (BALs), aiming to test how the broad absorption troughs seen in the rest-frame ultraviolet are linked to the narrow line region outflows seen in the rest-frame optical. We present new near-infrared spectra from Magellan/FIRE that cover [O III] in 12 quasars with $2.1 < z < 2.3$, selected to have strong outflow signatures in C IV λ1550. Combining with data from the literature, we build a sample of 73 BAL, 115 miniBAL, and 125 non-BAL quasars with $1.5 < z < 2.6$. The strength and velocity width of [O III] correlate strongly with the C IV emission properties, but no significant difference is seen in the [O III] emission-line properties between the BALs, non-BALs, and miniBALs once the dependence on C IV emission is taken into account. A weak correlation is observed between the velocities of C IV BALs and [O III] emission, which is accounted for by the fact that both outflow signatures correlate with the underlying C IV emission properties. Our results add to the growing evidence that BALs and non-BALs are drawn from the same parent population and are consistent with a scenario wherein BAL troughs are intermittent tracers of persistent quasar outflows, with a part of such outflow becoming optically thick along our line of sight for sporadic periods of time within which BALs are observed.

Key words: quasars: absorption lines – quasars: emission lines.

1 INTRODUCTION

Quasar-driven outflows are widely invoked in galaxy formation models in order to reproduce the observed properties of massive galaxies (e.g. Silk & Rees 1998; Springel, Di Matteo & Hernquist 2005; Bower et al. 2006; Harrison 2017). Luminous quasars are powerful sources of radiation, and if outflows from the active nucleus can propagate to galaxy scales then the energy in such an outflow would be enough to disrupt the interstellar medium of the host galaxy, preventing star formation and providing an explanation for the observed 'co-evolution' between supermassive black holes (SMBHs) and their hosts (Magorrian et al. 1998; Kormendy & Ho 2013).

High-velocity outflows have long been known to exist in many luminous quasars (King & Pounds 2015). Outflow velocities of many thousands of km s^{-1} are common and are believed to originate from material in a wide-angle outflowing disc wind (Murray et al. 1995; Giustini & Proga 2019). Such disc winds are now used to explain the blue asymmetric profiles of the high-ionization C IV λ1550 emission line (Richards et al. 2011; Matthews et al. 2020, 2023a; Stepney et al. 2023; Temple et al. 2023; Gillette & Hamann 2024). Up to 50 per cent of quasars exhibit strong, blueshifted absorption due to outflowing material present directly along the line of sight (Weymann et al. 1991; Hall et al. 2002; Allen et al. 2011; Rankine et al. 2020; Bischetti et al. 2023), and the outflow speeds in such 'broad absorption line' (BAL) quasars can exceed 50 000 km s^{-1} (Bruni et al. 2019; Rodríguez Hidalgo et al. 2020; Rodríguez Hidalgo & Rankine 2022).

Opinions differ as to whether the observed presence of BAL troughs represents a particular evolutionary phase in the quasar fuelling and outflow life cycle, or a special viewing angle, or whether instead BALs are a short, intermittent phase that all quasars will go through stochastically. To address this question, it is informative to consider complementary tracers of active galactic nucleus (AGN) winds that probe different phases and different locations in the outflow (Fiore et al. 2017). One popular probe of ionized gas kinematics in distant galaxies is the [O III] λλ4960, 5008[1] emission

★ E-mail: matthew.j.temple@durham.ac.uk

[1] Vacuum wavelengths are used throughout this paper: the [O III] doublet has λλ = 5006.8, 4958.9 in air and λλ = 5008.2, 4960.3 in vacuum.

doublet, which is usually inferred to originate in the 'narrow line region' on scales of up to ∼kiloparsecs (Baskin & Laor 2005; Dempsey & Zakamska 2018). Over recent years, many authors have studied the [O III] emission properties across different sub-classes of AGNs, finding that more luminous quasars generally show weaker [O III] emission that is broader and often blueshifted, suggesting that [O III] in luminous quasars is tracing AGN outflows in low-density ionized gas on scales that may be important for host galaxy feedback (e.g. Marziani et al. 2009, 2017; Liu et al. 2013; Harrison et al. 2014, 2016; Shen & Ho 2014; Zakamska & Greene 2014; Shen 2016; Bischetti et al. 2017; Temple et al. 2019; Kakkad et al. 2020; Villar Martín et al. 2020).

However, only a handful of studies have attempted to link quasar outflow signatures that are potentially probing different physical scales (e.g. Elvis 2000; Zamanov et al. 2002; Bruni et al. 2019; Xu et al. 2020; Yi et al. 2020). A holistic understanding of outflow properties probed using different diagnostics is the only way to fully understand the effect AGN feedback has on galaxy formation. Using a sample of ∼200 luminous non-BAL quasars, Coatman et al. (2019) found a correlation between the outflow kinematics of the rest-frame ultraviolet C IV λ1550 emission produced on $\lesssim$parsec scales (Fian et al. 2023; Hutsemékers et al. 2023; Shen et al. 2024) and the kinematics of the rest-frame optical [O III] $\lambda\lambda$4960, 5008 emission believed to originate on much larger scales. This result has also been found in smaller samples selected via X-rays (Vietri et al. 2020) and via their high luminosities in either mid-infrared (Vietri et al. 2018) or optical photometry (Deconto-Machado et al. 2023). Most importantly, these correlations are still seen even when the dependence of both C IV and [O III] on the quasar luminosity has been taken into account. These results are consistent with a scenario wherein nuclear outflows traced by the C IV emission are capable of propagating to galaxy-wide scales, where they would be able to return a significant amount of energy to the interstellar medium of their host galaxies.

To better understand how BAL outflows are linked to emission-line blueshifts, Rankine et al. (2020) measured the C IV emission-line parameters and BAL properties for ≃140 000 quasar spectra from the Sloan Digital Sky Survey (SDSS) Data Release 14 (DR14) quasar catalogue (Pâris et al. 2018). Spectrum reconstructions based on an independent component analysis (ICA) of a sample of non-BAL quasars allowed for the intrinsic C IV emission of both the BAL and non-BAL quasars to be robustly reconstructed and measured, even in the presence of extensive absorption. Rankine et al. (2020) found that the C IV emission properties of the BAL and non-BAL quasar populations were extremely similar, suggesting that BAL and non-BAL quasars represent different views of the same underlying quasar population. Additionally, BAL trough properties such as the maximum and minimum absorption velocities and the BALnicity index (BI, a measure of the amount of absorption; see Section 2.1 for the definition) were found to strongly correlate with C IV emission-line properties.

To further test the hypothesis put forward by Rankine et al. (2020), viz. that BALs and non-BALs are drawn from the same parent population, in this paper we investigate the narrow line region [O III] emission in a large sample of 73 BAL quasars and compare with the non-BAL population to test whether BALs show evidence for being in a special evolutionary phase. More precisely, in a model where the BAL outflows represent a specific phase in the quasar fuelling/outflow cycle, the extended narrow line region emission would be expected to differ significantly between the BAL and non-BAL quasars (Turnshek et al. 1997). The impact of the energetic BAL flows would reduce the emission from the static narrow line region although broader, more blueshifted [O III] emission may be seen (e.g. Zakamska et al. 2016). At a given C IV emission-line blueshift and equivalent width (EW), [O III] in the BAL quasars would have lower EW and be more blueshifted compared to the non-BALs. Alternatively, if BALs are stochastic phenomena that may appear intermittently for short periods of time while any galaxy is in a luminous quasar phase, then their [O III] properties should be very similar to non-BALs.

Previous near-infrared observations of $z > 1$ quasars have mostly focused on non-BAL quasars (e.g. Coatman et al. 2019), and so in Section 2 we present 12 new Magellan/FIRE spectra that were specifically targeted to observe the rest-frame optical [O III] in BAL quasars. We combine with archival data from the literature to build a sample of 73 BAL, 115 miniBAL, and 125 non-BAL quasars, as defined in Section 2.1. In Section 3, we then measure the [O III] strength and kinematics in our sample of BAL quasars, and compare the [O III] outflow signatures seen in the BAL, miniBAL, and non-BAL populations. We discuss our findings in Section 4 and summarize our conclusions in Section 5.

2 SAMPLE AND DATA

To investigate the link between the outflows seen in the rest-frame ultraviolet and rest-frame optical wavebands, we compile a sample of $1.5 < z < 2.6$ quasars with both SDSS observed-frame optical spectra (Section 2.1) and near-infrared spectra from various sources (Sections 2.2 and 2.3). To allow identification of broad absorption features up to 25 000 km s^{-1} bluewards of C IV, we require redshift $z > 1.56$ for objects with spectra from the BOSS spectrograph and $z > 1.67$ for objects with data from the original SDSS spectrograph (i.e. observations before the 'SDSS MJD' of 55000). The $z < 2.6$ criterion allows us to check for low-ionization Mg II broad absorption troughs in our final sample; no such low-ionization BAL troughs ('LoBALs') are found. To ensure reliable detection of absorption troughs in the SDSS spectra, we require the average signal-to-noise ratio per pixel to be ≥10, as the BAL fraction has been found to depend only weakly on the signal-to-noise ratio above this threshold [fig. 2 of Rankine et al. (2020), see also fig. 4 of Gibson et al. (2009)]. To ensure coverage of [O III], H β, and H α in the infrared *JHK* bands, we require either $1.56 < z < 1.65$ or $1.95 < z < 2.60$, to avoid emission lines falling in the regions of low atmospheric transparency between the *JHK* bands.

We measure the rest-frame ultraviolet monochromatic luminosity λL_λ at $\lambda = 3000$ Å (hereafter L_{3000}) by fitting a model spectral energy distribution (Temple, Hewett & Banerji 2021b) to the *griz* SDSS photometric data. Our final sample spans 8×10^{45} erg s^{-1} $< L_{3000} < 2 \times 10^{47}$ erg s^{-1}. The bolometric correction for each object is likely in the range $L_{\rm bol}/L_{3000} \approx 3$–10 (Temple et al. 2023, fig. 6), so all of the objects in our sample lie well above the $L_{\rm bol} \gtrsim 3 \times 10^{45}$ erg s^{-1} threshold that was suggested by Zakamska et al. (2016) as necessary for [O III] winds to contribute to quasar feedback.

Our compilation results in a total of 313 unique SDSS quasars with optical and near-infrared spectra covering the rest-frame 1400–2800 and 4800–6600 Å wavelength ranges, as shown in Figs 1 and 2. The majority of our sample (276/313) have $1.95 < z < 2.6$; only 37 quasars have $1.56 < z < 1.65$. We have verified that the results and conclusions of this paper would not change if we restricted our sample to $2 < z < 2.5$ and 10^{46} erg s^{-1} $< L_{3000} < 10^{47}$ erg s^{-1}. From our sample of 313 quasars, 125 objects show no C IV absorption exceeding ≈ 450 km s^{-1} in the rest-frame ultraviolet ('non-BALs'), 115 show mild absorption with trough widths >450 km s^{-1} that does not meet the strict definition of a BAL ('miniBAL' quasars), while

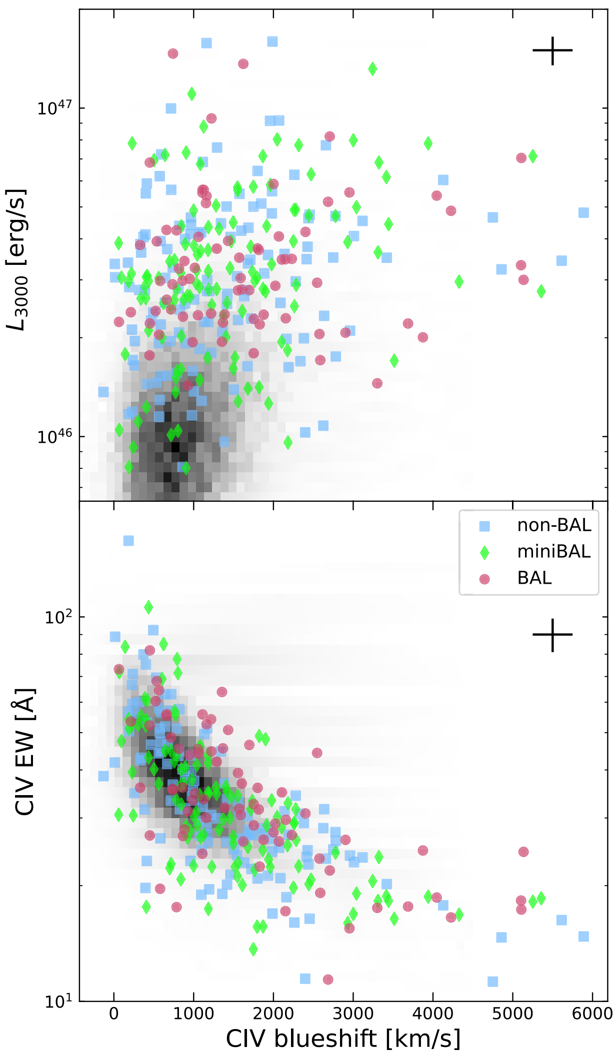

Figure 1. Distribution of our near-infrared sample as a function of rest-frame 3000 Å continuum luminosity (L_{3000}) and the C IV emission-line blueshift and EW. The typical uncertainty associated with each individual data point is shown by the black crosses in the upper right of each panel. In grey, we show the distribution of our parent sample of SDSS quasars with $1.5 < z < 2.6$ and signal-to-noise ratio >10. Our sample of objects with near-infrared data covers the mode of the SDSS population in emission-line space, while extending to brighter luminosities and larger C IV blueshifts to probe faster outflow signatures. The median ultraviolet continuum luminosity of each of our BAL, miniBAL, and non-BAL sub-samples is $L_{3000} = 3 \times 10^{46}$ erg s^{-1}, corresponding to $L_{\rm bol} \approx 1.5 \times 10^{47}$ erg s^{-1}.

73 sources are *bona fide* BAL quasars according to the definition of Weymann et al. (1991). All of our BAL quasars are so-called HiBAL systems that show no evidence for low-ionization absorption troughs.

We now describe in detail the data sets used, including the SDSS optical data (Section 2.1), 12 new near-infrared observations from the FIRE spectrograph (Section 2.2), and existing near-infrared spectra from the literature (Section 2.3). In Section 3, we then describe the methods used to analyse these spectra.

2.1 SDSS spectra and C IV measurements

We use the same C IV emission-line information as described in section 2.1 of Temple et al. (2023). In brief, we start with all quasars from the 16th and 17th data releases of SDSS (Lyke et al. 2020; Abdurro'uf et al. 2022). For this work, we consider only quasar spectra with mean signal-to-noise ratio (per 69 km s^{-1} pixel) ≥10 over the rest-frame interval of 1700–2200 Å. Each spectrum is reconstructed using the ICA scheme described by Rankine et al. (2020). A linear combination of 10 spectral ICA components is used to model the data, using an iterative routine to mask absorption features. This approach allows the underlying emission-line properties to be inferred consistently in both the BAL and non-BAL quasars. Examples of the SDSS data and corresponding ICA reconstructions are shown in Appendix A. We keep only ICA reconstructions with reduced-χ^2 <2. The C IV emission-line blueshift is measured as the Doppler shift of the median continuum-subtracted line flux, assuming a rest-frame wavelength of 1549.48 Å.

The uncertainty on the C IV blueshift is dominated by the systemic redshift uncertainty, which is $\lesssim$250 km s^{-1} for our $z \approx 2$ quasars (Hewett & Wild 2010). The uncertainties associated with our C IV emission-line EWs are dominated by the time variability of individual quasars, as for example investigated by Rivera et al. (2020) using a sample of high-cadence repeat spectroscopic observations. From fig. 9 of Rivera et al. (2020), we see that the C IV EW can vary by up to 20 per cent as a function of observation epoch.

BAL quasars are identified via the BALnicity index (BI; Weymann et al. 1991) and the absorption index (AI; Hall et al. 2002). The former is defined as

$$\mathrm{BI} = \int_{3000}^{25\,000} \left[1 - \frac{f(V)}{0.9}\right] C \,\mathrm{d}V, \quad (1)$$

with $C = 1$ when $f(V) < 0.9$ contiguously for at least 2000 km s^{-1}. $f(V) < 0.9$ is the continuum-normalized spectrum, in this case normalized by the reconstruction. The lower integration limit of 3000 km s^{-1} is set to remove any contribution of strong 'associated absorbers', while the upper 25 000 km s^{-1} limit avoids confusion with absorption of the Si IV λ1397 ion. The AI, on the other hand, includes absorption below 3000 km s^{-1} and requires $f(V) < 0.9$ contiguously for at least only 450 km s^{-1}:

$$\mathrm{AI} = \int_{0}^{25\,000} \left[1 - \frac{f(V)}{0.9}\right] C \,\mathrm{d}V. \quad (2)$$

There exists a bimodal distribution of log(AI) first observed by Knigge et al. (2008): one population of quasars has both AI > 0 and BI > 0, where, for the majority, the AI and BI are measuring the same absorption trough(s). The second population has AI > 0 but BI = 0 due to the presence of only narrow troughs, or broad troughs where a significant fraction of the absorption occurs below 3000 km s^{-1}. Here, we use 'miniBAL' to refer to the second AI > 0 population with BI = 0, i.e. quasars that have absorption troughs wider than 450 km s^{-1} without meeting the Weymann et al. (1991) definition of a BAL. Note that many of these 'miniBAL' systems are in fact narrow C IV doublet absorption features with $v_{\rm doublet} = 499$ km s^{-1} (see fig. 18 of Rankine et al. 2020), or 'line-locked' triplet systems that provide unambiguous evidence of radiation line driving playing an important role in AGN disc winds (Bowler et al. 2014; Lewis & Chelouche 2023).

2.2 New Magellan/FIRE spectra

We were awarded two nights on Magellan with FIRE (Simcoe et al. 2013) to obtain near-infrared spectra of quasars with unusual C IV emission-line properties (CN2020B-4; PI: Temple). Targets were selected from the SDSS DR14 quasar catalogue (Pâris et al. 2018; Rankine et al. 2020) to have redshifts $2.1 < z < 2.4$, ensuring

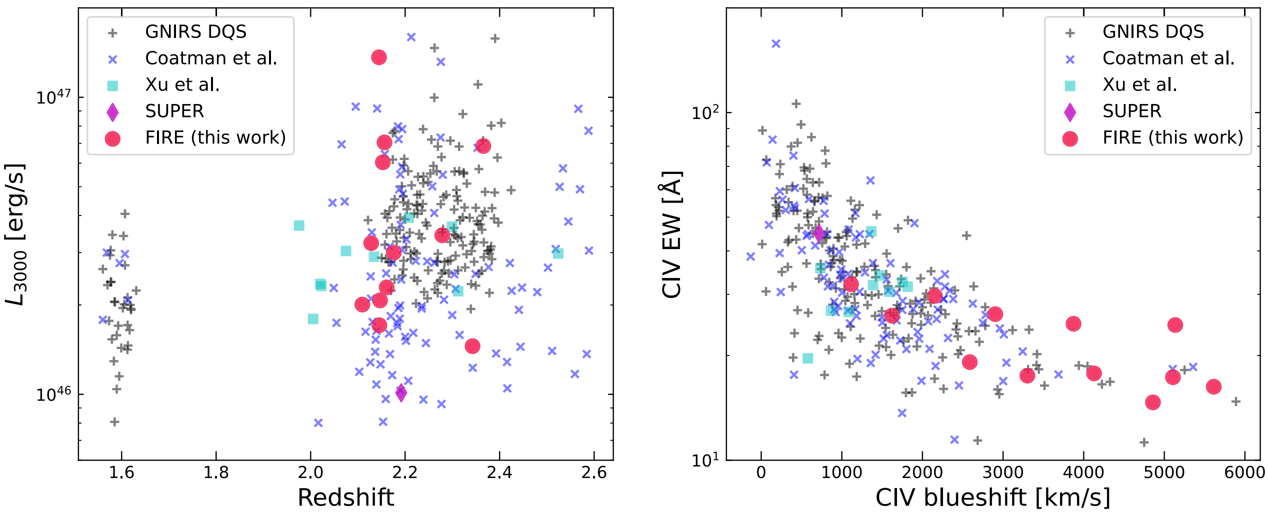

Figure 2. Distributions of redshift, luminosity, and C IV emission properties for the different near-infrared samples compiled in this work. Our new FIRE observations prioritized targets with larger C IV blueshifts, as such objects are rare in existing samples.

good observability of [O III] and H β in the H band and H α in the K band. We further required matches to VIKING (Edge et al. 2013), VHS (McMahon et al. 2013), UKIDSS-LAS (Lawrence et al. 2007), or 2MASS (Skrutskie et al. 2006) photometry with either $H < 17.1$ or $(J + K)/2 < 17.1$ to ensure good signal-to-noise ratio in the resulting near-infrared spectra. Targets were then prioritized based on their C IV properties: objects with large C IV blueshifts were preferred, as these are under-represented in existing samples. Targets were observed on the nights of 2022 January 02 and 03 using FIRE in Echelle mode with the 0.6 arcsec slit, which delivers $R = 6000$ spectra across 0.82–2.51 µm. Seeing was in the range of 0.5–0.9 arcsec with dark moon and no clouds. 12 science targets were observed, including 7 BALs and 3 non-BALs with C IV blueshift >2000 km s^{-1} and 2 filler targets (1 BAL and 1 non-BAL) with shorter exposures, as summarized in Table 1.

Spectra were reduced using the standard set-up in PYPEIT V1.11 (Prochaska et al. 2020; Westfall 2022). Targets were nodded along the slit in an ABBA dither pattern and combined in AA-BB groups for sky subtraction. Wavelength calibration was performed using night-sky emission features. Bright A0V stars observed directly before or after each science target were used for flux calibration. Spectra were then corrected for telluric absorption using a model grid. We show the reduced *JHK* spectra in Fig. 3: some residual telluric features can be observed around 20 000–20 150 Å, but H α and H β are clearly detected in each object. [O III] is clearly seen in e.g. J100711+053208, but in many objects there is strong Fe II emission in the H band and spectral modelling is required to deblend H β, [O III], and Fe II.

2.3 Existing near-infrared spectra

To complement our targeted observations with Magellan/FIRE, we also cross-match our parent sample of SDSS quasars to various catalogues from the literature to build a large sample of objects with coverage of C IV and [O III]. Starting from the SDSS sample described in Section 2.1, we look for near-infrared data from the GNIRS 'Distant Quasar Survey' (GNIRS-DQS; Matthews et al. 2021, 2023b), the previous compilation of Coatman et al. (2017, 2019), the X-Shooter programme described by Xu et al. (2019, 2020), and the SUPER survey (Circosta et al. 2018). For objects that have more than one near-infrared spectrum available, we keep only the spectrum with the highest signal-to-noise ratio in the 4800–5100 Å region that contains H β and [O III].

2.3.1 GNIRS data from the DQS

The Gemini/GNIRS-DQS (PI: Shemmer; Matthews et al. 2021, 2023b) is a large and long programme to obtain high signal-to-noise ratio near-infrared spectra for a large sample of SDSS quasars at $1.5 < z < 3.5$. Raw data were downloaded from the Gemini archive and reduced using PYPEIT. 190 objects from the GNIRS-DQS match to our sample of SDSS spectra.

2.3.2 Coatman et al. compilation

The largest previous catalogue of [O III] emission from near-infrared quasar spectra was described by Coatman et al. (2019). This compilation includes near-infrared spectra from WHT/LIRIS observations presented by Coatman et al. (2016), TRIPLESPEC and FIRE observations presented by Shen & Liu (2012) and Shen (2016), observations from the 'Quasars probing Quasars' project (Hennawi et al. 2006), and programmes from P200/TRIPLESPEC, VLT/SINFONI, and NTT/SOFI. The construction of this data set is described in full by Coatman et al. (2017). For the purposes of this investigation, we keep only spectra with median signal-to-noise ratio (per 69 km s^{-1} pixel) >3 across the rest-frame 4800–5100 Å region. 100 spectra from this catalogue with coverage of H β, [O III], and H α are matched to our SDSS sample.

2.3.3 X-Shooter data from Xu et al.

Xu et al. (2020) presented near-infrared observations of five BAL and two miniBAL quasars. These data were taken from a wider VLT/X-Shooter programme (PI: Benn), which observed a total of 20 quasars with rest-frame ultraviolet absorption features (Xu et al. 2019). 10 of these X-Shooter sources match to our SDSS parent sample. For each source, we downloaded the Phase 3 data products from the European Southern Observatory (ESO) archive. Each exposure was corrected

Table 1. Quasars with new near-infrared spectra obtained from Magellan/FIRE, as described in Section 2.2.

SDSS name	Classification	C IV EW (Å)	C IV blueshift (km s^{-1})	$z_{\rm uv}$	$i_{\rm SDSS}$ AB	J Vega	H Vega	K Vega	JHK source	$t_{\rm exp}$ (min)
J010754.95−095744.2	BAL	19.1	2587	2.146	18.55	17.37	–	16.14	VHS	90
J011934.27+052629.7	BAL	17.5	3302	2.343	18.93	17.48	16.77	15.99	UKIDSS	80
J014725.50−101438.9	non-BAL	17.8	4128	2.153	17.09	16.12	15.36	14.78	2MASS	30
J022943.90−003458.0	BAL	26.3	2903	2.147	18.19	17.01	16.51	15.68	VHS	60
J025345.28−080353.3	BAL	24.7	3874	2.109	18.41	17.26	–	15.96	VHS	90
J094748.06+193920.0	non-BAL	16.3	5613	2.279	17.78	16.98	16.46	15.78	2MASS	60
J100711.80+053208.8	BAL	26.1	1622	2.145	16.18	15.16	14.62	13.85	UKIDSS	20
J103546.02+110546.4	non-BAL	32.1	1115	2.365	17.26	15.77	15.10	14.23	UKIDSS	20
J120508.10+013455.8	BAL	29.7	2155	2.161	18.21	16.64	16.06	15.30	VIKING	40
J120550.19+020131.5	BAL	17.3	5108	2.156	16.94	16.02	15.61	15.00	VIKING	40
J121328.78−025617.8	BAL	24.5	5136	2.176	17.84	16.95	16.42	15.69	VIKING	60
J123647.13+185311.3	non-BAL	14.7	4859	2.128	17.64	16.69	–	15.32	2MASS	40

for telluric absorption using `molecfit` (Kausch et al. 2015; Smette et al. 2015). Where more than one exposure was present for a source, all such observations were combined to give the best signal-to-noise ratio spectrum for each quasar.

2.3.4 *SINFONI data from the SUPER survey*

The SUPER survey (Circosta et al. 2018; Kakkad et al. 2020; Vietri et al. 2020) is a VLT/SINFONI large programme (PI: Mainieri) designed to study AGN feedback at so-called cosmic noon, $z \approx 2$. Targets were selected from X-ray surveys to have redshifts $2 < z < 2.5$. We downloaded the DR1 data products from the ESO archive, which consist of the combined, flux-calibrated data cubes for 20 Type-1 AGNs presented by Kakkad et al. (2020). We extract 1D spectra from the SUPER data cubes using 0.6 arcsec apertures to match the slit width of our FIRE observations, and estimate 1D noise arrays from the pixel-to-pixel variations away from the source in each data cube. We find that one SUPER source with SINFONI $H + K$ data covering H β, [O III], and H α has SDSS data that meet the criteria described in Section 2.1.

3 METHODS AND RESULTS

3.1 Spectral modelling procedure

We use the open source code FANTASY[2] to simultaneously model the [O III], Fe II, and Balmer emission lines in each observed-frame optical spectrum from our sample of quasars. FANTASY is a PYTHON code for simultaneous multicomponent fitting of AGN spectra, described by Ilić et al. (2020), Ilić, Rakić & Popović (2023), and Rakić (2022). For our luminous (10^{46} erg s^{-1} $\lesssim L_{\rm bol} \lesssim 10^{48}$ erg s^{-1}) quasars, we do not include a host galaxy component. The Balmer lines (H α and H β, and where available H γ and H δ) are kinematically tied to have identical velocity profiles, with up to two broad and one narrow Gaussian components, although the relative normalization of each line is free to vary. A comprehensive set of Fe II emission blends is included as described by Ilić et al. (2023). We require coverage of H α to ensure robust modelling of the red wing of H β in objects with weak [O III] and strong Fe II blended around 4900–5100 Å.

We fit each spectrum twice: once with no [O III], and once with one broad and one narrow [O III] component. The 4960 and 5008 Å lines are constrained to have identical kinematics with the amplitudes tied in a 1:3 ratio. The Bayesian information criterion (BIC) is calculated for each fit. For quasars where the BIC is not improved by 10 or more when including [O III], we flag the [O III] component as not robustly detected and exclude the spectrum from our kinematic analysis. Many of these spectra would be inferred to have extremely weak (rest-frame) [O III] EW <1 Å. 228 objects from our sample of 313 quasars are judged to have robust [O III] detections: 57 BALs, 78 miniBALs, and 93 non-BALs. For these objects, we measure w_{80}, the velocity width containing 80 per cent of the total 5008 Å line flux, as is commonly used in the literature to quantify [O III] outflow signatures (Zakamska & Greene 2014; Coatman et al. 2019; Villar Martín et al. 2020).

3.2 Results

Our first observational result is the dependence of the [O III] EW on the C IV emission-line blueshift and EW, as shown in the bottom panels of Fig. 4. For objects with robust [O III] measurements, we show the w_{80} velocity width in the top panels of Fig. 4. Consistent with previous works (e.g. Coatman et al. 2019), we find that the [O III] properties are correlated with the ultraviolet C IV morphology. Objects with larger C IV blueshifts have weaker [O III] EW (Pearson's $r = -0.42$ and $p = 10^{-14}$) with broader [O III] w_{80} ($r = 0.45$ and $p = 10^{-12}$). Stronger C IV EW is correlated with stronger [O III] EW ($r = 0.65$ and $p = 10^{-39}$) and narrower [O III] w_{80} ($r = -0.34$ and $p = 10^{-7}$). When we compare our BAL, miniBAL, and non-BAL quasar samples, we see no difference in their [O III] emission, when the underlying dependence on the C IV emission properties is taken into account. In other words, we see no evidence for BAL or miniBAL quasars having different narrow line region properties when compared to their non-BAL counterparts.

We also see a weak trend with luminosity: objects with larger L_{3000} are more likely to show smaller [O III] EW ($r = -0.20$ and $p = 0.000\,37$) and broader [O III] w_{80} ($r = 0.23$ and $p = 0.000\,48$), consistent with previous works (Zakamska & Greene 2014; Coatman et al. 2019; Villar Martín et al. 2020). However, the dynamic range in luminosity spanned by the majority of our sample is relatively small (≈1 dex), and the correlation observed between [O III] and C IV is not a secondary effect driven by an underlying correlation with the intrinsic quasar luminosity (such as the Baldwin effect).

For our BAL and miniBAL quasar samples, we test whether the absorption trough properties are linked to the kinematics of the narrow line region traced by the [O III] emission. In Fig. 5, we show the [O III] EW and w_{80} as a function of absorption trough properties for both the miniBAL and the *bona fide* BAL populations.

[2] https://fantasy-agn.readthedocs.io

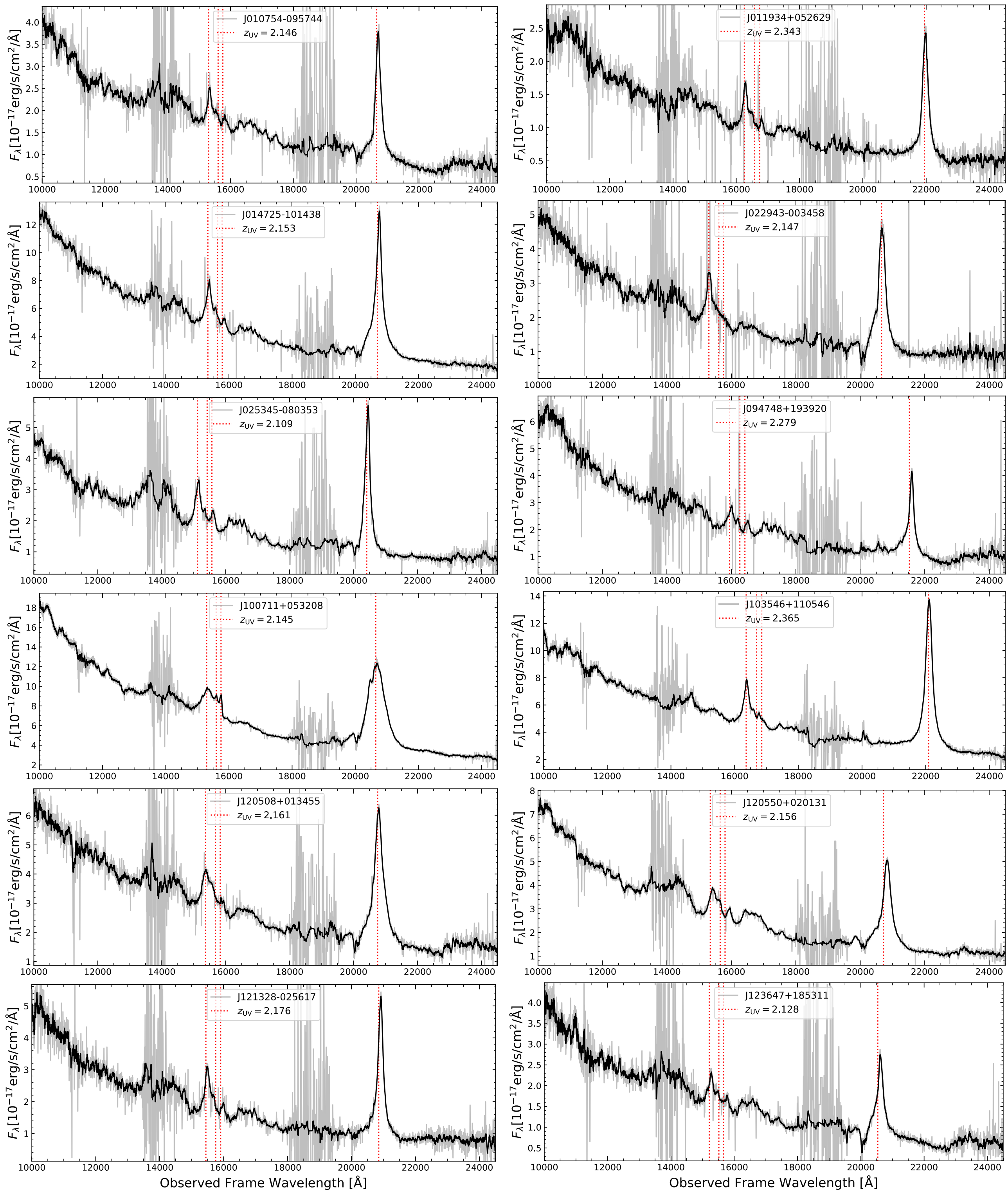

Figure 3. Magellan FIRE spectra for 12 quasars that are newly presented in this work (Section 2.2), with a resolution of 50 km s^{-1} ($R = 6000$). Grey shows the spectra, with a 9-pixel inverse variance weighted smooth in black. The expected wavelengths of H β, [O III], and H α are marked by vertical dotted red lines, assuming the redshifts estimated from the SDSS rest-frame ultraviolet spectra. The corresponding SDSS spectra are shown in Appendix A.

We show the Weymann et al. (1991) BI and Hall et al. (2002) AI, the absorption trough width (or median width, for quasars with more than one trough), and the fastest outflow velocity of the absorption trough (i.e. the fastest velocity contributing to the BI or AI measurements in equations 1 and 2), as these parameters have been seen to show the strongest correlations with C IV emission-line parameters (Rankine et al. 2020). We find a mild but statistically significant correlation between the maximum BAL trough velocity and the

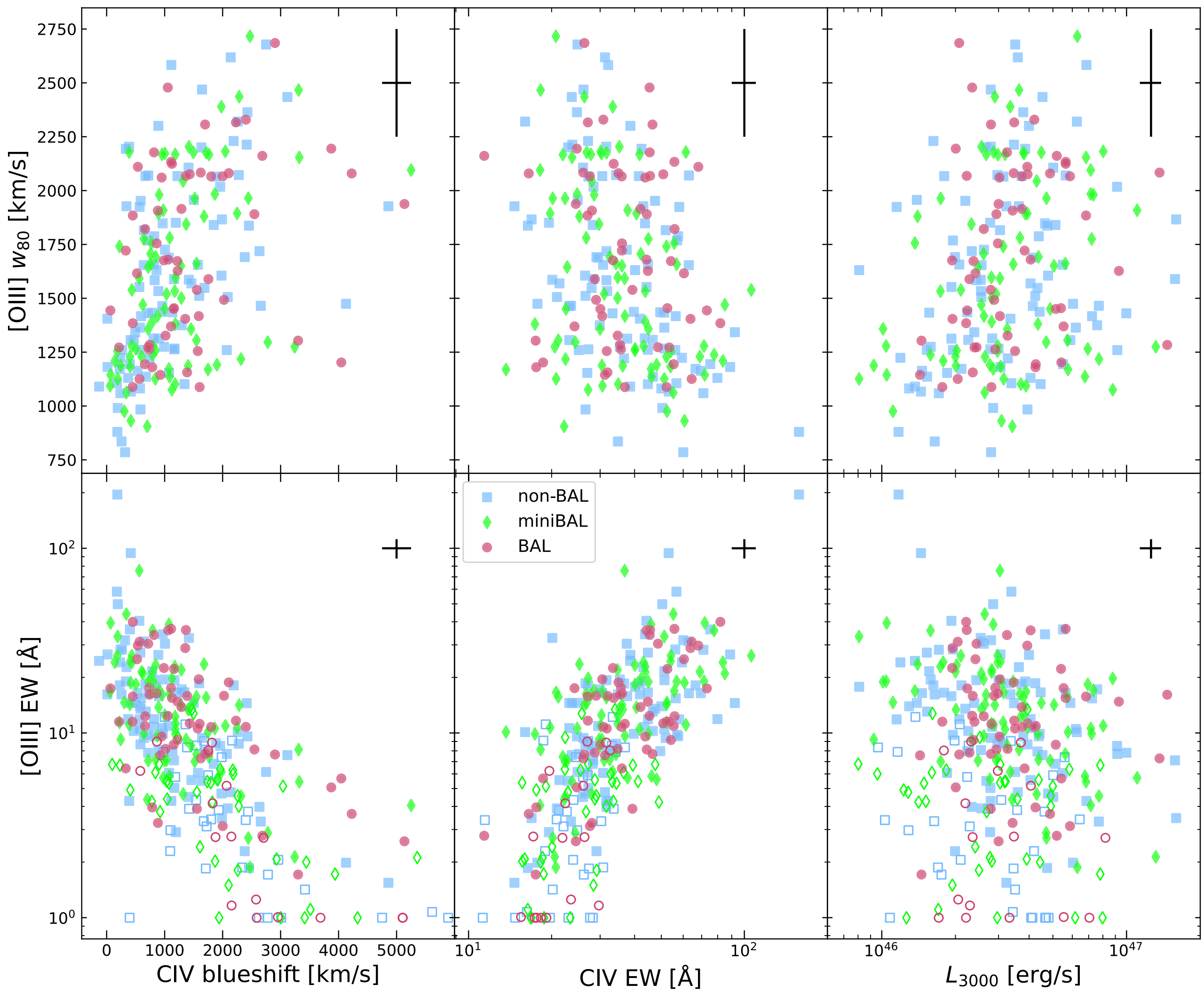

Figure 4. [O III] EW and w_{80} as a function of C IV properties and L_{3000}. The typical uncertainty associated with each individual data point is shown by the black crosses in the upper right of each panel. Open symbols indicate sources where ΔBIC < 10 when adding [O III] to the spectral model; these [O III] lines are not considered to be robustly detected and so we do not attempt to derive velocity width information. Objects with weaker [O III] are plotted at 1 Å EW for display purposes only. The [O III] strength and velocity width correlate with the C IV emission-line blueshift and EW, with the same trends observed in our samples of BAL, miniBAL, and non-BAL quasars.

[O III] w_{80} ($r = 0.37$ and $p = 0.004$). However, if we express the maximum trough velocity in units of the C IV emission-line blueshift the correlation with [O III] is not present, suggesting that the BAL is tracing the high-velocity tail of the C IV emission-line outflow, $v_{\rm max} \approx 10$ times the median C IV emission blueshift. None of the other BAL trough parameters computed by Rankine et al. (2020), such as the minimum trough velocity and velocity of the deepest part of the trough, is found to correlate with the [O III] measurements computed in this work.

4 DISCUSSION

The observational results presented in the previous section can be summarized as three key findings. *First*, larger C IV emission-line blueshift is observed to correlate with weaker C IV EW, weaker [O III] EW, and broader [O III] velocity width, confirming the correlations found in smaller samples by previous authors (Bachev et al. 2004; Marziani et al. 2017; Vietri et al. 2018, 2020; Coatman et al. 2019; Deconto-Machado et al. 2023). *Second*, BAL and miniBAL quasars do not show significant differences in their [O III] emission compared to their non-BAL counterparts. *And third*, while there is a mild correlation between the BAL outflow velocity and the [O III] velocity width, this is most likely driven by the fact that these parameters are both correlated with the underlying C IV emission-line kinematics (Coatman et al. 2019; Rankine et al. 2020).

In this section, we first discuss these findings in the context of previous work, and then explore possible interpretation.

4.1 Comparison with previous BAL investigations

We believe our investigation into the rest-frame optical [O III] properties of 73 BAL quasars represents the largest such sample available to date. Recently, Xu et al. (2020) conducted a similar investigation, measuring the [O III] strength and kinematics in a smaller sample of five BAL and two miniBAL quasars. Xu et al. (2020) selected their sample to have high-ionization Si IV BALs in

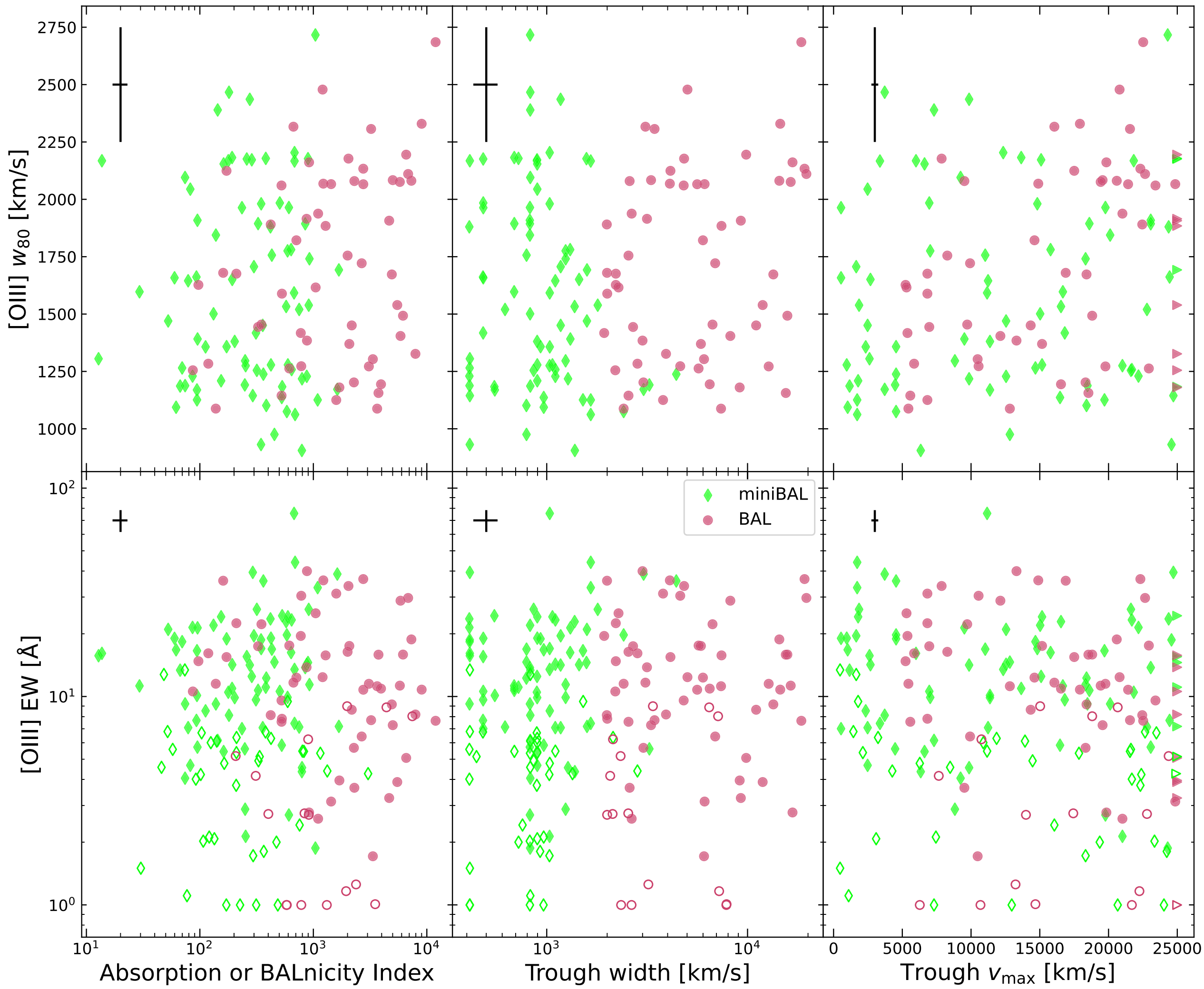

Figure 5. [O III] EW and velocity width as a function of C IV absorption properties. The typical uncertainty associated with each individual data point is shown by the black crosses in the upper left of each panel. As in Fig. 4, open symbols indicate objects where [O III] was not robustly detected in the near-infrared spectrum. For BAL quasars, we show the BI (equation 1) and the width and maximum velocity of the BAL trough. For miniBALs, we show the AI (equation 2) and the width and maximum velocity of the miniBAL trough. For objects with more than one trough, we plot the median trough width and the fastest maximum velocity. Our absorption-finding algorithm only searches up to 25 000 km s^{-1}, to avoid confusion with Si IV absorption, so the cluster of points on the right-hand edge of the right-hand panels (shown as triangles) could be considered lower limits on $v_{\rm max}$.

addition to C IV troughs, allowing them to infer constraints on the density and radius of the absorbing gas. They find that the electron number density derived for the absorbing material increases with decreasing [O III] EW.[3] They also find that the measured velocity widths have similar sizes in the BAL troughs and [O III] emission lines, and suggest that this is consistent with the [O III] emission and BAL absorption being 'different manifestations of the same wind'. Our [O III] velocity widths span a similar range to those found by Xu et al. (2020), with w_{80} in the range of 1000–2500 km s^{-1} and w_{90} in the range of 1000–3000 km s^{-1}. However, our BAL trough widths span a larger range, up to more than 20 000 km s^{-1}, and with our larger sample we do not find a significant correlation between the BAL trough widths and the [O III] velocity widths. Unlike Xu et al. (2020), we therefore do not believe that the [O III] emission and BAL absorption need to be tracing the same gas in each object, that is to say outflowing gas with the same density, ionization parameter, and location.

As this paper was going through the peer review process, Ahmed et al. (2024) was posted on the arXiv. They investigated 65 BAL quasars from the GNIRS-DQS and found no significant differences in their rest-frame optical spectra compared to a control sample of non-BAL quasars. Our results are in agreement with Ahmed et al. (2024), although we note that our larger sample size and new Magellan/FIRE data together also allow us to investigate the [O III] emission in a statistical sample of BALs with more extreme C IV blueshifts $\gtrsim$ 2500 km s^{-1}.

In this work, we have focused on high-ionization BAL quasars, which do not show absorption troughs from low-ionization lines such as Mg II λ2800 and Al III λ1860. Quasars with such LoBALs can be identified at lower redshifts when Mg II or Al III is present in the SDSS observed-frame optical spectrum (Voit, Weymann & Korista 1993). Schulze et al. (2017) presented near-infrared observations of 22 LoBALs at $1.3 < z < 2.5$, finding no enhancement in [O III] outflow

[3] Xu et al. report $L_{[\rm O\,III]}/L_{\rm bol}$, which is closely related to the EW.

signature compared to the wider non-BAL population. Matthews, Knigge & Long (2017) also found no difference in distribution of [O III] EWs in 58 LoBALs at $0.35 < z < 0.83$, when compared to wider SDSS quasar population at the same redshift. Our results are consistent with these works to the extent that neither our high-ionization BAL quasars nor their low-ionization BAL quasars show any significant difference from the non-BAL population in terms of their optical [O III] emission, suggesting that the narrow line region properties are not significantly impacted by the presence of a broad absorption feature in the rest-frame ultraviolet.

4.2 Implications for quasar winds and feedback

This investigation was motivated (in part) by the idea that if BAL and non-BAL quasars are members of two distinct AGN populations with different disc winds, driving ionized gas outflows with differing powers, then we might expect BALs and non-BALs to show differences in their narrow line region (as traced by the [O III] strength and kinematics). However, this is true only if the length of the BAL phase is comparable to the time taken to affect the narrow line region. Estimates of quasar lifetimes are typically of the order of 1–10 Myr (Khrykin et al. 2021), which together with the significant (∼10–40 per cent) observed BAL fraction (Allen et al. 2011) means that if the BAL phenomenon was a single evolutionary phase then it would typically last at least ∼0.1 Myr. In this time, a BAL outflow travelling at 10 000 km s^{-1} would travel ∼1 kpc, meaning that we would expect it to reach the scales that we are probing with [O III]. In Section 3.2, we found that the BAL, miniBAL, and non-BAL quasar populations show no significant differences in their narrow line region [O III] properties. Our results therefore suggest that the BAL phenomenon is not a distinct, long-lived evolutionary phase in the cycle of SMBH growth, at least within the context of luminous quasar activity.

One possible interpretation could instead be that BAL outflows do not do anything to affect the [O III]-emitting gas in luminous quasars – either suggesting that the kinetic power contained in BAL outflows is negligible or that they are entrained in a particular geometry that means that they are directed away from the narrow line region gas. This would imply either that BAL outflows are not important for quasar feedback, which is unlikely given that photoionization models of BAL troughs suggest that at least some BALs carry significant kinetic power (Arav et al. 2018; Xu et al. 2019), or that the [O III]-emitting region is not tracing the impact of quasar-mode outflows on the interstellar medium of the AGN's host galaxy.

On the other hand, if we assume that BAL outflows should affect the narrow line region, then the similarity seen in the BAL and non-BAL quasars would suggest that the observation of a BAL trough is an intermittent, but recurring phenomenon during the luminous quasar phase of the SMBH growth cycle. There is a growing body of work suggesting that BAL troughs can vary on relatively short time-scales, which would support this hypothesis (Gibson et al. 2008, 2010; Hamann et al. 2008; Capellupo et al. 2011, 2013; Filiz Ak et al. 2012, 2013; Grier et al. 2015; McGraw et al. 2017; De Cicco et al. 2018; Rogerson et al. 2018; Hemler et al. 2019; Mishra et al. 2021; Vietri et al. 2022; Aromal, Srianand & Petitjean 2023). In other words, our results would be consistent with a scenario where BAL troughs are an intermittent tracer of a persistent quasar outflow (which could be the wind traced by the C IV emission blueshift), where a part of the outflow along our line of sight becomes optically thick for short periods of time when a broad absorption trough is observed. This scenario would explain the correlations observed between the C IV and [O III] outflow signatures: luminous quasars that drive winds on nuclear scales are also able to drive outflows on much larger scales, with stochastic parts of the wind sometimes producing absorption features that do not correlate directly with the properties of the narrow line region outflow. The general properties of such nuclear winds would then be governed by the shape and strength of the ionizing quasar continuum, which is in turn set by the SMBH mass and accretion rate (Temple et al. 2023). This scenario would also explain the fact that BAL and non-BAL quasars have no significant difference in their underlying C IV emission (Rankine et al. 2020) or their sublimation-temperature dust emission [section 4.3 of Temple et al. (2021a), see also Saccheo et al. (2023)], but a further element would be required to explain the differences in radio properties of the BAL and non-BAL populations observed by Petley et al. (2022, 2024), especially as the radio emission in AGNs is often found to be linked with the [O III] properties (e.g. Jarvis et al. 2021).

5 CONCLUSIONS

We have measured the rest-frame optical [O III] $\lambda\lambda$4960, 5008 emission in a sample of 73 BAL, 115 miniBAL, and 125 non-BAL quasars at $1.56 < z < 2.6$ with high-quality near-infrared spectroscopic data. Our key observational results are as follows:

Table 2. Description of columns for the supplementary data file available at MNRAS online.

Column name	Description	Units	Example entry
`Name`	SDSS name	–	J000730.94−095831.9
`RA`	Right ascension	Decimal degrees	1.878 937 691 054 3467
`Dec`	Declination	Decimal degrees	−9.975 545 336 959 057
`z`	Redshift	–	2.224
`L3000`	Logarithm of 3000 Å luminosity	dex (erg s^{-1})	46.47
`Classification`	[BAL, miniBAL, non-BAL]	–	BAL
`CIV_EW`	C IV EW	Ångström	35.99
`CIV_blue`	C IV blueshift	km s^{-1}	861.4
`BI_BI`	BALnicity index (equation 1)	km s^{-1}	2003.4
`BI_VMAX`	BAL trough maximum velocity	km s^{-1}	8271.8
`BI_WIDTH`	BAL trough median width	km s^{-1}	2553.1
`AI_AI`	Absorption index (equation 2)	km s^{-1}	3348.6
`AI_VMAX`	AI trough maximum velocity	km s^{-1}	16 815.9
`AI_WIDTH`	AI trough median width	km s^{-1}	1311.5
`O3_EW`	[O III] EW	Ångström	16.38
`O3_w80`	[O III] 80 per cent velocity width	km s^{-1}	1754.8
`O3_w90`	[O III] 90 per cent velocity width	km s^{-1}	2254.1

(i) The properties of [O III] λ5008 and C IV λ1550 emission are connected: larger C IV emission-line blueshift and weaker C IV EW correlate with weaker [O III] EW and broader [O III] velocity structure. These correlations are not driven solely by changes in the 3000 Å continuum luminosity.

(ii) BAL, miniBAL, and non-BAL quasars show no significant differences in their [O III] emission: all three sub-samples show the same correlations described in (i).

(iii) In BAL quasars, the maximum absorption trough velocity shows a weak correlation with the [O III] velocity width, but this is fully explained by the dependence of both quantities on the C IV emission-line blueshift. When the BAL outflow velocities are normalized by the C IV blueshift, we find no correlations between the [O III] emission kinematics and the C IV BAL trough parameters.

Our results disfavour a scenario where (high-ionization) BAL quasars are a special, long-lived evolutionary phase in which more powerful (cf. non-BAL quasars) winds are able to propagate into the interstellar medium of their host galaxies, and either clear out or alter the kinematics of this medium. Instead, our results are consistent with a scenario in which BAL troughs are an intermittent, stochastic phenomenon that all luminous quasars with persistent outflowing winds (traced by both [O III] and C IV emission) are likely to undergo. This is consistent with observations of BAL trough variability on time-scales of only months to years, and supports the scenario favoured by Rankine et al. (2020) where BALs and non-BALs are members of the same underlying quasar population.

NOTE ADDED IN PROOF

Leighly et al. (2022, 2024) have recently investigated the rest-frame optical properties in a rare sub-class of BAL quasars which show absorption from iron species, the so-called FeLoBAL quasars. Leighly et al. find a dramatic difference in the [O III] EWs of FeLoBAL quasars when compared to the LoBAL, HiBAL and non-BAL populations. However, consistent with our discussion in Section 4.1, they find no significant differences between the [O III] EWs of LoBAL and non-BAL quasars.

ACKNOWLEDGEMENTS

MJT acknowledges funding from a FONDECYT postdoctoral fellowship (3220516) and from STFC (ST/X001075/1). ALR acknowledges support from UKRI (MR/T020989/1). MB and JHM acknowledge funding from the Royal Society via University Research Fellowships (URF/R/221003 and URF/R1/221062). CR acknowledges support from Fondecyt Regular grant 1230345 and ANID BASAL project FB210003.

This research made use of ASTROPY,[4] a community-developed core PYTHON package and an ecosystem of tools and resources for astronomy (Astropy Collaboration 2013, 2018, 2022), MATPLOTLIB (Hunter 2007), NUMPY (Harris et al. 2020), FANTASY[5] (Ilić et al. 2020, 2023; Rakić 2022), and PYPEIT,[6] a PYTHON package for semi-automated reduction of astronomical slit-based spectroscopy (Prochaska et al. 2020). MJT thanks Dalia Baron and Christina Eilers for advice in using PYPEIT, Xinfeng Xu for advice on the X-Shooter sample, Vincenzo Mainieri for advice on the SUPER data, Brandon Matthews for advice on GNIRS-DQS, and Bartolomeo Trefoloni for access to data from Trefoloni et al. (2023). We thank the anonymous referee for a thorough report, which helped to improve the manuscript. MJT would also like to thank Kate Grier for a useful discussion on BAL variability.

This paper includes new data gathered with the 6.5-m Magellan Telescopes located at Las Campanas Observatory, Chile through CNTAC programme CN2020B-4 (PI: Temple). These observations were originally scheduled for 2020 July; we thank CNTAC for carrying over the programme to 2022 January.

This paper uses data from the SUPER survey (Circosta et al. 2018) based on data products created from observations collected at the European Organisation for Astronomical Research in the Southern Hemisphere under ESO programme 196.A-0377. This paper also uses X-Shooter data from ESO programmes 087.B-0229, 090.B-0424, 091.B-0324, and 092.B-0267. This research has made use of the services of the ESO Science Archive Facility.

This paper uses data from GNIRS-DQS (Matthews et al. 2021, 2023b), based on observations obtained at the international Gemini Observatory with programme IDs GN-2017B-LP-16, GN-2018A-LP-16, GN-2018B-LP-16, GN-2019A-LP-16, GN-2019B-LP-16, GN-2020A-LP-16, and GN-2020B-LP-16. Gemini is a programme of NSF's NOIRLab, which is managed by the Association of Universities for Research in Astronomy (AURA) under a cooperative agreement with the National Science Foundation on behalf of the Gemini Observatory partnership: the National Science Foundation (United States), National Research Council (Canada), Agencia Nacional de Investigación y Desarrollo (Chile), Ministerio de Ciencia, Tecnología e Innovación (Argentina), Ministério da Ciência, Tecnologia, Inovações e Comunicações (Brazil), and Korea Astronomy and Space Science Institute (Republic of Korea). This work was enabled by observations made from the Gemini North telescope, located within the Maunakea Science Reserve and adjacent to the summit of Maunakea. We are grateful for the privilege of observing the Universe from a place that is unique in both its astronomical quality and its cultural significance.

Funding for the SDSS-IV has been provided by the Alfred P. Sloan Foundation, the U.S. Department of Energy Office of Science, and the Participating Institutions. SDSS-IV acknowledges support and resources from the Center for High-Performance Computing at the University of Utah. The SDSS website is www.sdss.org.

DATA AVAILABILITY

The optical spectroscopic data underlying this article are available from SDSS.[7] New Magellan/FIRE infrared spectra will be made available via the Strasbourg astronomical data center (CDS). A file with the emission-line measurements used in this work is included as supplementary data. The file contains a table with 313 rows, 1 for each quasar, and columns as described in Table 2.

REFERENCES

Abdurro'uf et al., 2022, ApJS, 259, 35
Ahmed H. et al., 2024, ApJ, 968, 77
Allen J. T., Hewett P. C., Maddox N., Richards G. T., Belokurov V., 2011, MNRAS, 410, 860
Arav N., Liu G., Xu X., Stidham J., Benn C., Chamberlain C., 2018, ApJ, 857, 60
Aromal P., Srianand R., Petitjean P., 2023, MNRAS, 522, 6374
Astropy Collaboration, 2013, A&A, 558, A33

[4] http://www.astropy.org
[5] https://fantasy-agn.readthedocs.io
[6] https://pypeit.readthedocs.io/en/latest/
[7] https://www.sdss4.org/dr17/

Astropy Collaboration, 2018, AJ, 156, 123
Astropy Collaboration, 2022, ApJ, 935, 167
Bachev R., Marziani P., Sulentic J. W., Zamanov R., Calvani M., Dultzin-Hacyan D., 2004, ApJ, 617, 171
Baskin A., Laor A., 2005, MNRAS, 358, 1043
Bischetti M. et al., 2017, A&A, 598, A122
Bischetti M. et al., 2023, ApJ, 952, 44
Bower R. G., Benson A. J., Malbon R., Helly J. C., Frenk C. S., Baugh C. M., Cole S., Lacey C. G., 2006, MNRAS, 370, 645
Bowler R. A. A., Hewett P. C., Allen J. T., Ferland G. J., 2014, MNRAS, 445, 359
Bruni G. et al., 2019, A&A, 630, A111
Capellupo D. M., Hamann F., Shields J. C., Halpern J. P., Barlow T. A., 2013, MNRAS, 429, 1872
Capellupo D. M., Hamann F., Shields J. C., Rodríguez Hidalgo P., Barlow T. A., 2011, MNRAS, 413, 908
Circosta C. et al., 2018, A&A, 620, A82
Coatman L., Hewett P. C., Banerji M., Richards G. T., 2016, MNRAS, 461, 647
Coatman L., Hewett P. C., Banerji M., Richards G. T., Hennawi J. F., Prochaska J. X., 2017, MNRAS, 465, 2120
Coatman L., Hewett P. C., Banerji M., Richards G. T., Hennawi J. F., Prochaska J. X., 2019, MNRAS, 486, 5335
De Cicco D., Brandt W. N., Grier C. J., Paolillo M., Filiz Ak N., Schneider D. P., Trump J. R., 2018, A&A, 616, A114
Deconto-Machado A., del Olmo Orozco A., Marziani P., Perea J., Stirpe G. M., 2023, A&A, 669, A83
Dempsey R., Zakamska N. L., 2018, MNRAS, 477, 4615
Edge A., Sutherland W., Kuijken K., Driver S., McMahon R., Eales S., Emerson J. P., 2013, The Messenger, 154, 32
Elvis M., 2000, ApJ, 545, 63
Fian C. et al., 2023, A&A, 678, A108
Filiz Ak N. et al., 2012, ApJ, 757, 114
Filiz Ak N. et al., 2013, ApJ, 777, 168
Fiore F. et al., 2017, A&A, 601, A143
Gibson R. R. et al., 2009, ApJ, 692, 758
Gibson R. R., Brandt W. N., Gallagher S. C., Hewett P. C., Schneider D. P., 2010, ApJ, 713, 220
Gibson R. R., Brandt W. N., Schneider D. P., Gallagher S. C., 2008, ApJ, 675, 985
Gillette J., Hamann F., 2024, MNRAS, 528, 6425
Giustini M., Proga D., 2019, A&A, 630, A94
Grier C. J. et al., 2015, ApJ, 806, 111
Hall P. B. et al., 2002, ApJS, 141, 267
Hamann F., Kaplan K. F., Rodríguez Hidalgo P., Prochaska J. X., Herbert-Fort S., 2008, MNRAS, 391, L39
Harris C. R. et al., 2020, Nature, 585, 357
Harrison C. M. et al., 2016, MNRAS, 456, 1195
Harrison C. M., 2017, Nat. Astron., 1, 0165
Harrison C. M., Alexander D. M., Mullaney J. R., Swinbank A. M., 2014, MNRAS, 441, 3306
Hemler Z. S. et al., 2019, ApJ, 872, 21
Hennawi J. F. et al., 2006, ApJ, 651, 61
Hewett P. C., Wild V., 2010, MNRAS, 405, 2302
Hunter J. D., 2007, Comput. Sci. Eng., 9, 90
Hutsemékers D., Sluse D., Savić Đ., Richards G. T., 2023, A&A, 672, A45
Ilić D. et al., 2020, A&A, 638, A13
Ilić D., Rakić N., Popović L. Č., 2023, ApJS, 267, 19
Jarvis M. E. et al., 2021, MNRAS, 503, 1780
Kakkad D. et al., 2020, A&A, 642, A147
Kausch W. et al., 2015, A&A, 576, A78
Khrykin I. S., Hennawi J. F., Worseck G., Davies F. B., 2021, MNRAS, 505, 649
King A., Pounds K., 2015, ARA&A, 53, 115
Knigge C., Scaringi S., Goad M. R., Cottis C. E., 2008, MNRAS, 386, 1426
Kormendy J., Ho L. C., 2013, ARA&A, 51, 511
Lawrence A. et al., 2007, MNRAS, 379, 1599
Leighly K. et al.., 2022, ApJ, 935, 92
Leighly K.et al., 2024, ApJ, 966, 87
Lewis T. R., Chelouche D., 2023, ApJ, 945, 110
Liu G., Zakamska N. L., Greene J. E., Nesvadba N. P. H., Liu X., 2013, MNRAS, 436, 2576
Lyke B. W. et al., 2020, ApJS, 250, 8
Magorrian J. et al., 1998, AJ, 115, 2285
Marziani P., Negrete C. A., Dultzin D., Martínez-Aldama M. L., Del Olmo A., D'Onofrio M., Stirpe G. M., 2017, Front. Astron. Space Sci., 4, 16
Marziani P., Sulentic J. W., Stirpe G. M., Zamfir S., Calvani M., 2009, A&A, 495, 83
Matthews B. M. et al., 2021, ApJS, 252, 15
Matthews B. M. et al., 2023b, ApJ, 950, 95
Matthews J. H. et al., 2023a, MNRAS, 526, 3967
Matthews J. H., Knigge C., Higginbottom N., Long K. S., Sim S. A., Mangham S. W., Parkinson E. J., Hewitt H. A., 2020, MNRAS, 492, 5540
Matthews J. H., Knigge C., Long K. S., 2017, MNRAS, 467, 2571
McGraw S. M. et al., 2017, MNRAS, 469, 3163
McMahon R. G., Banerji M., Gonzalez E., Koposov S. E., Bejar V. J., Lodieu N., Rebolo R., VHS Collaboration, 2013, The Messenger, 154, 35
Mishra S., Vivek M., Chand H., Joshi R., 2021, MNRAS, 504, 3187
Murray N., Chiang J., Grossman S. A., Voit G. M., 1995, ApJ, 451, 498
Pâris I. et al., 2018, A&A, 613, A51
Petley J. W. et al., 2022, MNRAS, 515, 5159
Petley J. W. et al., 2024, MNRAS, 529, 1995
Prochaska J. et al., 2020, J. Open Source Softw., 5, 2308
Rakić N., 2022, MNRAS, 516, 1624
Rankine A. L., Hewett P. C., Banerji M., Richards G. T., 2020, MNRAS, 492, 4553
Richards G. T. et al., 2011, AJ, 141, 167
Rivera A. B., Richards G. T., Hewett P. C., Rankine A. L., 2020, ApJ, 899, 96
Rodríguez Hidalgo P., Khatri A. M., Hall P. B., Haas S., Quintero C., Khatu V., Kowash G., Murray N., 2020, ApJ, 896, 151
Rodríguez Hidalgo P., Rankine A. L., 2022, ApJ, 939, L24
Rogerson J. A., Hall P. B., Ahmed N. S., Rodríguez Hidalgo P., Brandt W. N., Filiz Ak N., 2018, ApJ, 862, 22
Saccheo I. et al., 2023, A&A, 671, A34
Schulze A. et al., 2017, ApJ, 848, 104
Shen Y. et al., 2024, ApJS, 272, 26
Shen Y., 2016, ApJ, 817, 55
Shen Y., Ho L. C., 2014, Nature, 513, 210
Shen Y., Liu X., 2012, ApJ, 753, 125
Silk J., Rees M. J., 1998, A&A, 331, L1
Simcoe R. A. et al., 2013, PASP, 125, 270
Skrutskie M. F. et al., 2006, AJ, 131, 1163
Smette A. et al., 2015, A&A, 576, A77
Springel V., Di Matteo T., Hernquist L., 2005, MNRAS, 361, 776
Stepney M., Banerji M., Hewett P. C., Temple M. J., Rankine A. L., Matthews J. H., Richards G. T., 2023, MNRAS, 524, 5497
Temple M. J. et al., 2023, MNRAS, 523, 646
Temple M. J., Banerji M., Hewett P. C., Coatman L., Maddox N., Peroux C., 2019, MNRAS, 487, 2594
Temple M. J., Banerji M., Hewett P. C., Rankine A. L., Richards G. T., 2021a, MNRAS, 501, 3061
Temple M. J., Hewett P. C., Banerji M., 2021b, MNRAS, 508, 737
Trefoloni B. et al., 2023, A&A, 677, A111
Turnshek D. A., Monier E. M., Sirola C. J., Espey B. R., 1997, ApJ, 476, 40
Vietri G. et al., 2018, A&A, 617, A81
Vietri G. et al., 2020, A&A, 644, A175
Vietri G. et al., 2022, A&A, 668, A87
Villar Martín M., Perna M., Humphrey A., Castro Rodríguez N., Binette L., Pérez González P. G., Mateos S., Cabrera Lavers A., 2020, A&A, 634, A116
Voit G. M., Weymann R. J., Korista K. T., 1993, ApJ, 413, 95
Westfall K., 2022, PypeIt: Version 1.11.0, available at https://doi.org/10.5281/zenodo.7235644
Weymann R. J., Morris S. L., Foltz C. B., Hewett P. C., 1991, ApJ, 373, 23

Xu X., Arav N., Miller T., Benn C., 2019, ApJ, 876, 105
Xu X., Zakamska N. L., Arav N., Miller T., Benn C., 2020, MNRAS, 495, 305
Yi W. et al., 2020, ApJ, 893, 95
Zakamska N. L. et al., 2016, MNRAS, 459, 3144
Zakamska N. L., Greene J. E., 2014, MNRAS, 442, 784
Zamanov R., Marziani P., Sulentic J. W., Calvani M., Dultzin-Hacyan D., Bachev R., 2002, ApJ, 576, L9

SUPPORTING INFORMATION

Supplementary data are available at *MNRAS* online.

O3_results_MNRAS_Apr2024.fits

APPENDIX A: SDSS DATA

For each of the 12 quasars with new Magellan/FIRE spectra presented in Section 2.2 (Fig. 3), the SDSS rest-frame ultraviolet spectra and corresponding ICA reconstructions are shown in Fig. A1.

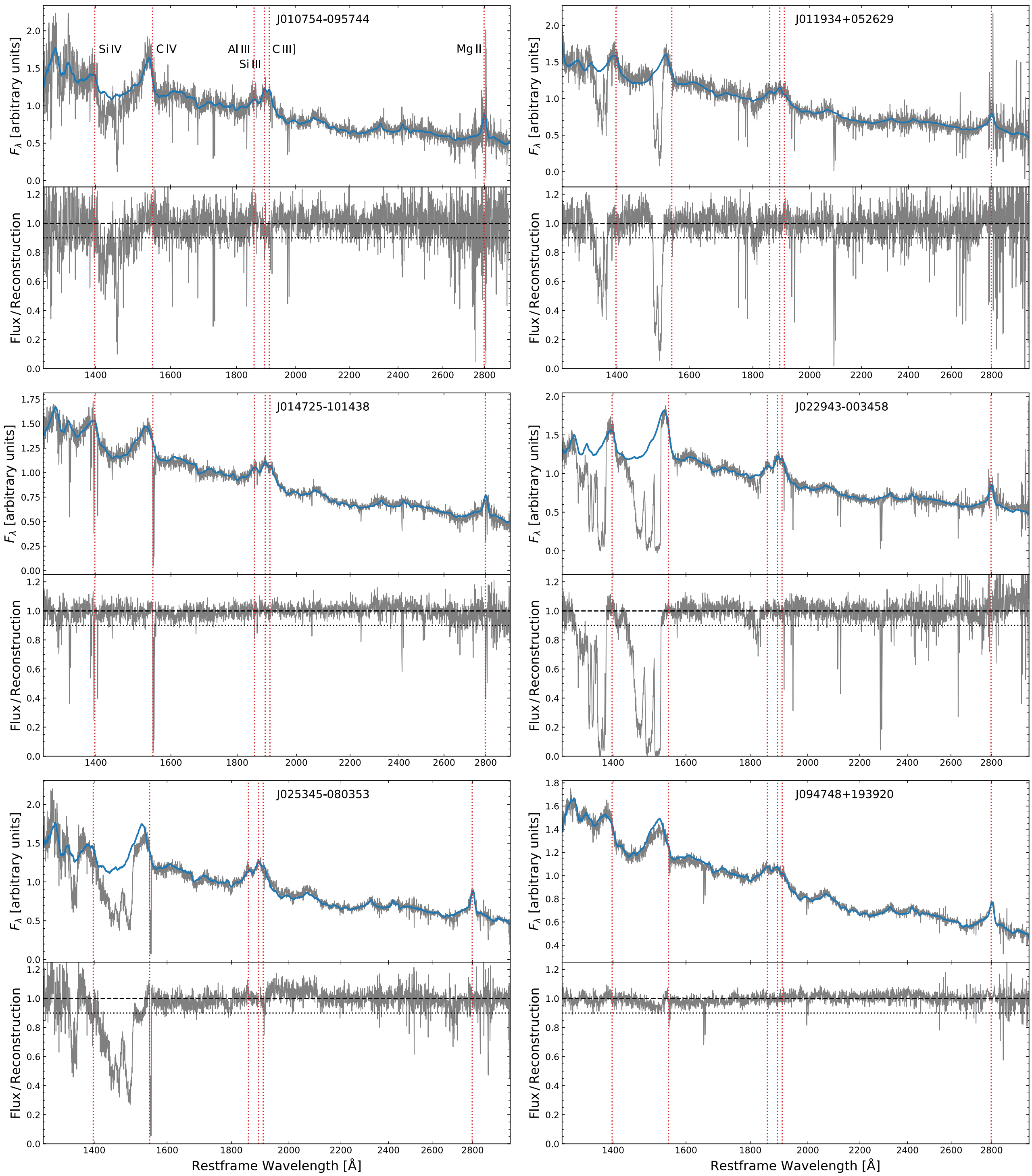

Figure A1. Examples of the rest-frame ultraviolet measurements used in this work. Red vertical dotted lines show the rest-frame wavelengths of Si IV, C IV, Al III, Si III], C III], and Mg II. Top panels show the SDSS spectra in grey and corresponding ICA spectral reconstruction in blue. Absorption features are iteratively masked when modelling the observed data, allowing the ICA to reconstruct the unabsorbed pixels. Lower panels show the ratio of the observed and reconstructed flux, with the dotted horizontal line showing the 0.9 threshold used to detect absorption features. BAL quasars are required to have at least 2000 km s^{-1} contiguous absorption (i.e. flux/reconstruction <0.9) starting from at least 3000 km s^{-1} bluewards of C IV (equation 1). Objects with slower and/or narrower absorption features broader than 450 km s^{-1} are classed as 'miniBALs' (equation 2); otherwise, the quasar is considered a 'non-BAL'.

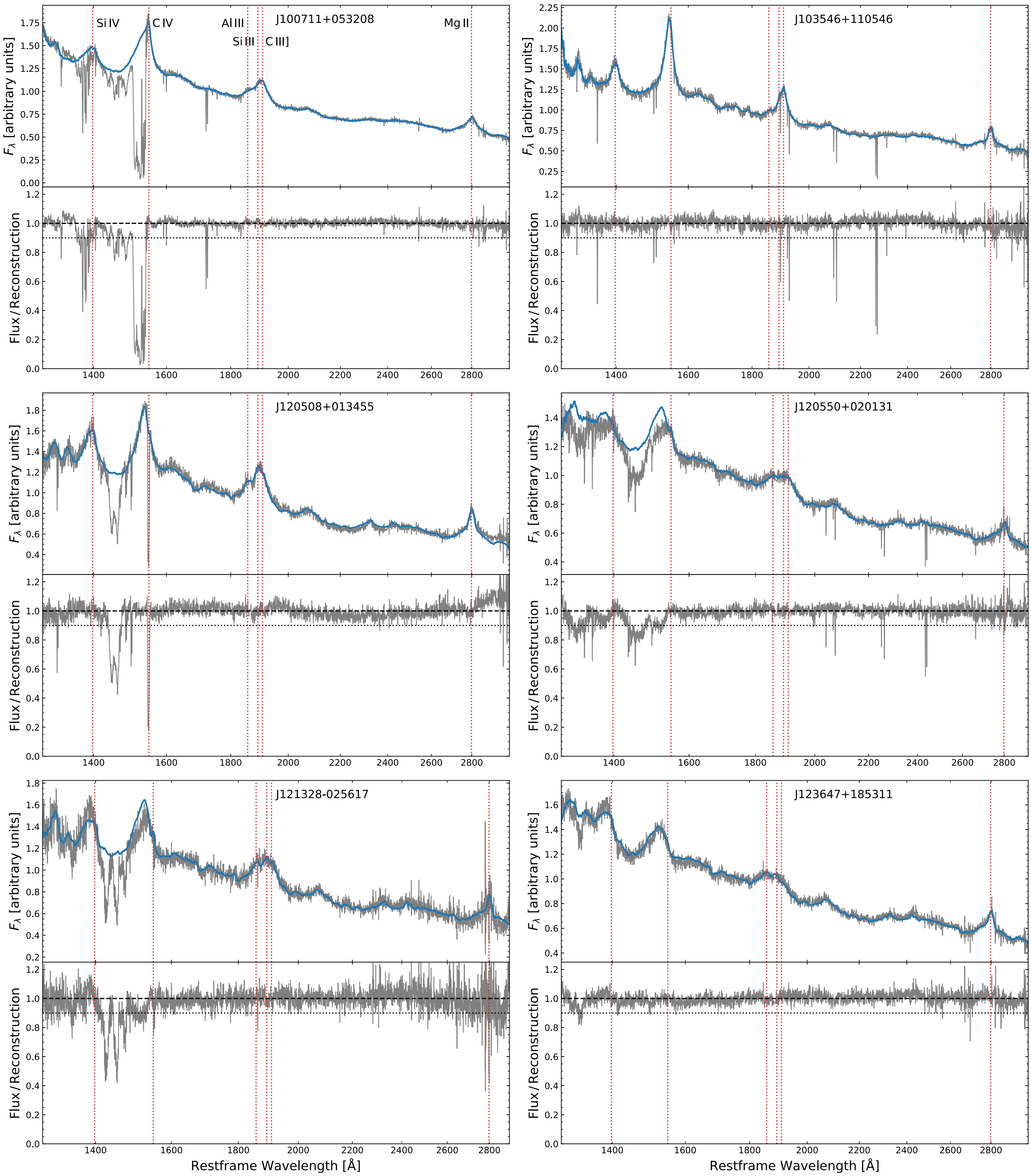

Figure A1. *continued.*

This paper has been typeset from a TEX/LATEX file prepared by the author.